J. Fluid Mech. (2007), *vol.* 583, *pp.* 161–187.
doi:10.1017/S0022112007006131 Printed in the United Kingdom

Bragg scattering by a line array of small cylinders in a waveguide. Part 1. Linear aspects

YILE LI[1]† AND CHIANG C. MEI[2]

[1]Department of Mechanical Engineering, Massachusetts Institute of Technology, Cambridge, MA 02139, USA

[2]Department of Civil and Environmental Engineering, Massachusetts Institute of Technology, Cambridge, MA 02139, USA

(Received 8 November 2006 and in revised form 4 February)

Motivated by potential applications for offshore airports supported on vertical piles, we report a theory of wave diffraction by a periodic array of circular cylinders. The simple case of normal incidence on a rectangular array is studied here, which is equivalent to a line array along the centre of a long channel. An asymptotic theory is developed for cylinders much smaller than the incident wavelength, which is comparable to the cylinder spacing. Focus is on Bragg resonance near which scattering is strong. A combination of the method of multiple scales and the Bloch theorem leads to simple evolution equations coupling the wave envelopes. Dispersion of transient wave envelopes is investigated. Scattering of detuned waves by a large but finite number of cylinders is investigated for frequencies in and outside the band gap. Quantitative accuracy is assessed by comparisons with numerical computations via finite elements. The analytical theory prepares the ground for nonlinear studies and may facilitate future inclusion of real-fluid effects such as vortex shedding.

1. Introduction

Because land area is limited in many highly populated countries, offshore airports are likely to become more common. Osaka and Tokyo have airstrips built on man-made islands, and research has been conducted on floating airstrips in deep sea, similar in concept to the Mobile Offshore Bases (MOB) contemplated for military purposes. Future designs will probably include airstrips rigidly supported above the water surface by a periodic array of piles. As in the construction of oil-drilling platforms, the pile diameter should be small compared to both the spacing and the dominant wavelength. Prediction of wave forces on these piles requires accurate modelling of scattering (linear and nonlinear) and vortex shedding. Of these two hydrodynamic aspects, wave scattering can be dealt with in the framework of potential theory; vortex shedding can only be treated by incorporating empirical information.

As the pile spacing is likely to be comparable with the incident wavelength, Bragg resonance, a common feature of wave propagation through a periodic medium, is relevant. Some basic physics of Bragg resonance can be revealed by studying an infinite array of scatterers, in particular, the band structure of the dispersion relation (see e.g. Kittel 2004 and Aschcroft & Mermin 1976 on solid-state physics and Joannopoulos, Meade & Winn 1995 on photonic crystals). When a monochromatic

† Present address: Shell International Exploration & Production Inc., Houston, TX 77025, USA.

incident wavetrain strikes a periodic array of finite extent, multiple scattering can excite Bragg resonance if the frequency falls within one of the band gaps.

Many solution techniques exist in the theory of multiple scattering in linear wave physics. Mathematical aspects of exact methods for general geometries and frequencies can be found in Linton & Evans (2001) or Martin (2006). For water waves Ohkusu (1970), Srokosz & Evans (1979) and Evans (1990) have developed approximate theories for a number of vertical cylinders spaced at a distance D much greater than the wavelength, i.e. $kD \gg 1$. Approximations are also possible when the wavelength is much greater than the scatterer dimension and spacing (e.g. Hu & Chan (2005)). In this limit the physical consequence is an averaged index of refraction. For numerically accurate (or exact) predictions without restrictions of spacing and scatterer size, most existing strategies reduce to the numerical solution of truncated series or of boundary-integral equations (see Maystre, Saillard & Tayeb 2001, for a recent survey for electromagnetic waves). For a periodic array of identical circular cylinders, Spring & Monkmeyer (1974) used local polar coordinates and expressed the scattered waves as eigenfunction expansions. The boundary conditions on the cylinders led to an infinite matrix equation for the expansion coefficients, to be solved numerically. By using Graf's addition theorem for Bessel functions, Linton & Evans (1990) improved the convergence of the series and expedited the computation of the matrix system. For the scattering of an obliquely incident wave by a large number of cylinders in a periodic and linear array, Maniar & Newman (1997) used integral equations and predicted the resonance of trapped modes found by Callan, Linton & Evans (1991). In the mathematically similar problem of acoustics, Linton & Martin (2004) gave a theory for a semi-infinite array of small sound-soft (perfectly absorbing) cylinders. Detailed numerical results revealing the resonance of trapped modes were described for head-sea diffraction by Linton, Porter & Thompson (2007). For three-dimensional scattering involving more general geometry, a powerful semi-numerical method has been devised by Kagemoto & Yue (1986) for finite depth and extended by Goo & Yoshida (1990), Peter & Meylan (2004) and Peter, Meylan & Linton (2006).

Of special interest is the case of resonant scattering, which is difficult to treat by numerical schemes designed for general frequencies. For an infinite line of circular cylinders Linton & Thompson (2007) gave a theory for general incidence and obtained numerical results at exact resonances based on series-expansion solutions. An approximate theory has been given by Kriegsmann (2004) for the normal incidence on an infinite grating with narrow openings between rectangular blocks. Large transmission is found at resonances. In the case of small scatterers (compared with the spacing and the wavelength), asymptotic theories are possible by the perturbation method of multiple scales. The heuristic basis is that a scattered wave can be resonated to the level of the incident wave only if the number of small scatterers is large. Hence two sharply contrasting length scales must exist. For surface water waves over parallel sand bars Mei (1985) derived envelope equations† governing the slow and coupled evolution of incident and reflected waves near and at Bragg resonance. Theoretical extensions with experimental confirmations have been reported by Hara & Mei (1987); Mei, Hara & Naciri (1988); Rey, Guazzelli & Mei (1996) and Naciri & Mei (1988). There is evidence that these asymptotic theories can be reasonably accurate even beyond the immediate neighbourhood of resonance, when compared with calculations based on fuller theories (Miles & Chamberlain 1998).

† Similar results are known as the coupled-mode equations in one-dimensional optics of layered media (Yariv & Yeh 1984).

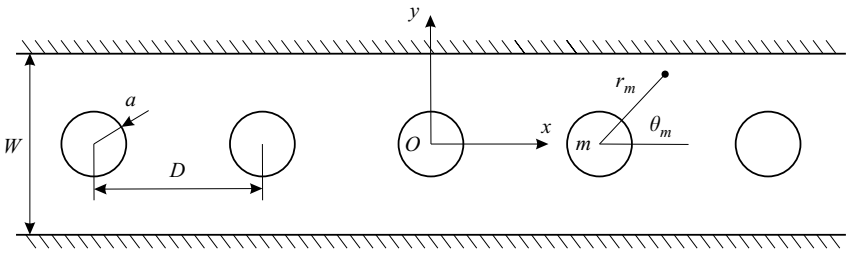

FIGURE 1. A line of periodic circular cylinders in a channel.

In this two-part series we shall ignore vortex shedding and develop an asymptotic theory of one-dimensional wave propagation through a linear array of vertical cylinders along the centreline of a long channel. The mathematical problem is two-dimensional and is identical to that for a planar array of cylinders along perpendicular lines in the channel with the incident wave along one set of lines. Focus will be on the neighbourhood of Bragg resonance in which the physics and the practical implications are the most interesting. The sea depth H will be taken to be constant and the cylinder radius a is small compared to the spacing D, the channel width W and the characteristic wavelength, i.e.

$$ka = \mu \ll 1, \quad (kD, kW, kH) = O(1). \tag{1.1}$$

The wave steepness is assumed to be small $kA \ll 1$. As the cumulative effect of Bragg resonance can alter the leading-order physics after a distance much longer than a typical wavelength, the asymptotic method of multiple-scale expansions widely used in mechanics will be employed to derive equations for the slow variation of the wave envelopes. Analytical solutions will be obtained for physical insight. This Part 1 is restricted to linear aspects. Numerical accuracy will be verified by a finite element method. The nonlinear effects of long waves generated by two trains of short waves of nearly equal frequencies will be studied in Part 2. Two-dimensional propagation through a planar array of periodic cylinders will be reported elsewhere.

2. Linearized boundary value problem

Referring to figure 1, we consider a plane wave incident upon a long line of bottom-mounted vertical cylinders of radius a in the central plane of an open channel of width W and depth H. A large but finite number of cylinders are spaced at equal distance D apart along the channel axis. Let a Cartesian coordinate system be chosen such that the (x, y)-plane coincides with the still free surface and z points vertically upward. The coordinates of the cylinder centres are $x_m^o = mD$, $y_m^o = 0$, $m = 0, \pm 1, \pm 2, \ldots, \pm N$. Near cylinder m, the local polar coordinates (r_m, θ_m) are defined by

$$x - x_m^o = r_m \cos\theta_m, \quad y = r_m \sin\theta_m. \tag{2.1}$$

Let the fluid be incompressible and inviscid and the flow be irrotational. A plane wave of amplitude A_0 and angular frequency ω arrives from $x \sim -\infty$. The velocity potential is governed by Laplace's equation

$$\nabla^2 \Phi + \frac{\partial^2 \Phi}{\partial z^2} = 0, \tag{2.2}$$

in the fluid, where ∇^2 is the horizontal Laplacian. Restricting to infinitesimal waves,

the linearized dynamic and kinematic free-surface conditions are

$$\frac{\partial \Phi}{\partial t} + g\zeta = 0, \qquad \frac{\partial \zeta}{\partial t} = \frac{\partial \Phi}{\partial z}, \qquad z = 0, \tag{2.3}$$

where ζ is the free-surface elevation. These can be combined to give

$$\frac{\partial^2 \Phi}{\partial t^2} + g\frac{\partial \Phi}{\partial z} = 0 \qquad \text{on} \quad z = 0. \tag{2.4}$$

We also require no-flux boundary conditions on all cylinder surfaces,

$$\frac{\partial \Phi}{\partial r_m} = 0, \qquad r_m = a, \quad m = 0, \pm 1, \pm 2, \ldots, \pm N, \tag{2.5}$$

on the channel sidewalls,

$$\frac{\partial \Phi}{\partial y} = 0, \qquad y = \pm\frac{W}{2}, \tag{2.6}$$

and on the seabed,

$$\frac{\partial \Phi}{\partial z} = 0, \qquad z = -H, \tag{2.7}$$

Since the geometry is D-periodic on the short scale comparable to the wavelength, Bloch's theorem, well-known in crystallography and solid state physics (Kittel 2004), must apply to the potential on the short scale, i.e. Φ is of the form

$$\Phi = F_+(x, y, z, t)\mathrm{e}^{\mathrm{i}kx} + F_-(x, y, z, t)\,\mathrm{e}^{-\mathrm{i}kx} \tag{2.8}$$

where $F_\pm(x, y, z, t)$ are D-periodic in x, although they may vary slowly over the much longer scale parametrically. In addition the radiation condition is required so that the scattered waves are outgoing from the region of scatterers.

It will be shown in Part 2 that the linearized free-surface conditions are valid if the wave steepness is small enough that $\epsilon = kA_0 \leqslant O(\mu^2)$, implying $A_0/a = kA_0/ka = \epsilon/\mu \leqslant O(\mu) \ll 1$.

3. Multiple-scale expansions

As is well known, when the spacing D between successive scatterers is half-integral multiples of the incident wavelength, i.e.

$$kD = n_B\pi \tag{3.1}$$

where n_B is a positive integer, constructive interference gives rise to strong reflection. Since the reflection coefficient from a single cylinder is of $O(\mu^2)$, the accumulated effects over N cylinders becomes of $O(1)$ when $N = O(1/\mu^2)$, i.e. over the distance $x = O(1/k\mu^2)$. It follows that strong reflection evolves over the dimensionless length scale $k(x, y) = O(1/\mu^2)$. The multiple-scale perturbation method (Nayfeh 1973; Cole & Kevorkian 1981) is therefore appropriate.

As we shall also examine the physical effect of small detuning in wavenumber $\mu^2 K$ and frequency $\mu^2\Omega$, which are related by the dispersion relation, the following slow time and space coordinates are introduced:

$$x_1 = \mu^2 x, \qquad t_1 = \mu^2 t. \tag{3.2}$$

In terms of these, detuning and its effects are represented by the slow variation of the complex amplitudes, while (3.1) implies perfect tuning at the leading order only. The wave potential is expanded as follows:

$$\Phi = \{\phi_1\,\mathrm{e}^{-\mathrm{i}\omega t} + \text{c.c.}\} + \mu^2\{\phi_2\,\mathrm{e}^{-\mathrm{i}\omega t} + \text{c.c.}\} + \cdots, \tag{3.3}$$

where $\phi_1, \phi_2, \ldots$ are functions of $x, y, z; x_1, t_1$, and c.c. denotes the complex conjugate of the preceding term.

At the leading order $O(\mu^0)$, ϕ_1 is governed by

$$\nabla^2\phi_1 + \frac{\partial^2\phi_1}{\partial z^2} = 0 \qquad \text{in the fluid domain,} \tag{3.4}$$

$$\frac{\partial\phi_1}{\partial z} - \frac{\omega^2}{g}\phi_1 = 0 \qquad \text{on} \quad z = 0, \tag{3.5}$$

$$\frac{\partial\phi_1}{\partial y} = 0 \qquad \text{on} \quad y = \pm\frac{W}{2}, \tag{3.6}$$

$$\frac{\partial\phi_1}{\partial z} = 0 \qquad \text{on} \quad z = -H. \tag{3.7}$$

Owing to the smallness of the cylinder radius relative to the wavelength, scattering is of $O(\mu^2)$ and unimportant. Thus ϕ_1 represents solely the sum of the incident and the reflected waves, in anticipation of the accumulated effect of resonance over a long scale. In particular the error by ignoring the no-flux boundary condition on the cylinders is of $O(\mu^2)$, and will be corrected at the next order by ϕ_2. Thus the formal non-trivial solution of the first-order homogeneous problem consists simply of two plane waves:

$$\phi_1(x, y; x_1, t_1) = Z(z)(A^+(x_1, t_1)\,\mathrm{e}^{\mathrm{i}kx} + A^-(x_1, t_1)\,\mathrm{e}^{-\mathrm{i}kx}), \tag{3.8}$$

where $A^+(x_1, t_1)$ and $A^-(x_1, t_1)$ are respectively the unknown amplitudes of the incident and reflected waves. $Z(z)$ describes the vertical profile

$$Z(z) = -\frac{\mathrm{i}g}{2\omega}\frac{\cosh k(z+H)}{\cosh kH}. \tag{3.9}$$

The frequency ω is related to the wavenumber k by the dispersion relation:

$$\omega^2 = gk\tanh kH, \tag{3.10}$$

where k satisfies the Bragg condition (3.1). Since A^+ and A^- are independent of x, Bloch's condition is trivially satisfied.

4. Second-order problem

Upon substituting (3.3) and (3.8) into (2.2) and (2.4)–(2.7), we obtain the boundary value problem for the second-order potential:

$$\nabla^2\phi_2 + \frac{\partial^2\phi_2}{\partial z^2} = -2\frac{\partial^2\phi_1}{\partial x\,\partial x_1} \qquad \text{in the fluid domain,} \tag{4.1}$$

$$\frac{\partial\phi_2}{\partial z} - \frac{\omega^2}{g}\phi_2 = \frac{2\mathrm{i}\omega}{g}\frac{\partial\phi_1}{\partial t_1} \qquad \text{on} \quad z = 0, \tag{4.2}$$

$$\frac{\partial\phi_2}{\partial r_m} = -\frac{1}{\mu^2}\frac{\partial\phi_1}{\partial r_m} \qquad \text{on} \quad r_m = a, \quad m = 0, \pm1, \ldots, \tag{4.3}$$

$$\frac{\partial\phi_2}{\partial y} = 0 \qquad \text{on} \quad y = \pm\frac{W}{2}, \tag{4.4}$$

$$\frac{\partial\phi_2}{\partial z} = 0 \qquad \text{on} \quad z = -H. \tag{4.5}$$

In addition we require that ϕ_2 satisfies Bloch's condition (2.8).

Note that the small error introduced earlier by neglecting the boundary condition on the cylinder is now remedied at the second order by (4.3). Despite the appearance of the large factor $1/\mu^2$, it will be seen shortly that both sides of the condition are of comparable order. From (3.8) we obtain by differentiation and Taylor expansion,

$$\begin{aligned}
-\frac{1}{\mu^2}\frac{\partial\phi_1}{\partial r_m}\bigg|_{r_m=a} &= -\frac{Z(z)}{\mu^2}\frac{\partial}{\partial r_m}\left\{A^+ \mathrm{e}^{\mathrm{i}k(x_m^o + r_m\cos\theta_m)} + A^- \mathrm{e}^{-\mathrm{i}k(x_m^o + r_m\cos\theta_m)}\right\} \\
&= -\frac{Z(z)}{\mu^2}\left\{A^+ \mathrm{e}^{\mathrm{i}kx_m^o}\mathrm{i}k\cos\theta_m\,\mathrm{e}^{\mathrm{i}ka\cos\theta_m} - A^- \mathrm{e}^{-\mathrm{i}kx_m^o}\mathrm{i}k\cos\theta_m\,\mathrm{e}^{-\mathrm{i}ka\cos\theta_m}\right\} \\
&= -kZ(z)\left\{\mathrm{e}^{\mathrm{i}kx_m^o}A^+\left[\frac{\mathrm{i}\cos\theta_m}{\mu^2} - \frac{ka\cos^2\theta_m}{\mu^2} + \frac{O((ka)^2)}{\mu^2}\right]\right. \\
&\quad \left. + \mathrm{e}^{-\mathrm{i}kx_m^o}A^-\left[\frac{-\mathrm{i}\cos\theta_m}{\mu^2} - \frac{ka\cos^2\theta_m}{\mu^2} + \frac{O((ka)^2)}{\mu^2}\right]\right\}. \qquad (4.6)
\end{aligned}$$

Since $ka = \mu$ and $kx_m^o = mkD = mn_B\pi$ according to (3.1), it follows that $\mathrm{e}^{\mathrm{i}mkD} = \mathrm{e}^{-\mathrm{i}mkD}$. Equation (4.6) may be written

$$\begin{aligned}
-\frac{1}{\mu^2}\frac{\partial\phi_1}{\partial r_m}\bigg|_{r_m=a} &= -\mathrm{e}^{\mathrm{i}mkD}kZ(z)\left\{A^+\left[\frac{\mathrm{i}\cos\theta_m}{\mu^2} - \frac{1+\cos 2\theta_m}{2\mu}\right]\right. \\
&\quad \left. + A^-\left[-\frac{\mathrm{i}\cos\theta_m}{\mu^2} - \frac{1+\cos 2\theta_m}{2\mu}\right]\right\} + O(\mu^0). \qquad (4.7)
\end{aligned}$$

The large boundary value on the right is effective only over a small cylinder of circumference of order $ka = O(\mu)$ relative to the wavelength, hence the integrated effect is of the same order as ϕ_2.

The second-order velocity potential is governed by an inhomogeneous Laplace equation (4.1) subject to the inhomogeneous condition (4.2) on the free surface and (4.3) on the cylinder surface. In view of linearity, we decompose ϕ_2 into two parts:

$$\phi_2 = \phi_2^{(1)} + \phi_2^{(2)}, \qquad (4.8)$$

where $\phi_2^{(1)}$ satisfies the homogeneous Laplace equation and free-surface condition and the inhomogeneous cylinder surface boundary condition. No condition is imposed on the channel walls. On the other hand $\phi_2^{(2)}$ must satisfy the remaining inhomogeneous conditions. In particular it must satisfy

$$\frac{\partial\phi_2^{(1)}}{\partial y} + \frac{\partial\phi_{21}^{(2)}}{\partial y} = 0 \qquad \text{on} \quad y = \pm\frac{W}{2} \qquad (4.9)$$

on the channel walls. Let us derive the solution for the first part.

4.1. *Solution for* $\phi_2^{(1)}$

The potential $\phi_2^{(1)}$ is defined by the following boundary value problem:

$$\nabla^2\phi_2^{(1)} + \frac{\partial^2\phi_2^{(1)}}{\partial z^2} = 0 \qquad \text{in the fluid domain,} \qquad (4.10)$$

$$\frac{\partial\phi_2^{(1)}}{\partial z} - \frac{\omega^2}{g}\phi_2^{(1)} = 0 \qquad \text{on} \quad z = 0, \qquad (4.11)$$

$$\frac{\partial\phi_2^{(1)}}{\partial z} = 0 \qquad \text{on} \quad z = -H, \qquad (4.12)$$

$$\frac{\partial \phi_2^{(1)}}{\partial r_m} = -kZ(z)\,\mathrm{e}^{\mathrm{i}mkD}\left\{A^+\left(\frac{\mathrm{i}\cos\theta_m}{\mu^2} - \frac{1+\cos 2\theta_m}{2\mu}\right)\right.$$
$$\left. + A^-\left(-\frac{\mathrm{i}\cos\theta_m}{\mu^2} - \frac{1+\cos 2\theta_m}{2\mu}\right)\right\} \quad \text{on} \quad r_m = a, \quad m = 0, \pm 1, \pm 2, \ldots \pm N. \tag{4.13}$$

Bloch's condition (2.8) is required. The no-flux condition on the sidewalls $y = \pm W/2$ will be imposed on the sum $\phi_2^{(1)} + \phi_2^{(2)}$ later but not on $\phi_2^{(1)}$.

We now propose a series solution of the following form:

$$\phi_2^{(1)} = Z(z)\chi(x, y), \tag{4.14}$$

where

$$\chi(x, y) = \sum_{m=-N}^{N} \left\{\left[B_m^Y Y_0(kr_m) + B_m^J J_0(kr_m)\right] + \left[C_m^Y Y_1(kr_m) + C_m^J J_1(kr_m)\right]\cos\theta_m \right.$$
$$\left. + \left[D_m^Y Y_2(kr_m) + D_m^J J_2(kr_m)\right]\cos 2\theta_m\right\} \tag{4.15}$$

so that $\phi_2^{(1)}$ satisfies the Laplace equation (4.10) and the boundary conditions (4.11) and (4.12). Since for a small argument

$$Y_0'(ka) \sim \frac{2}{\pi ka}, \quad Y_1'(ka) \sim \frac{2}{\pi k^2 a^2}, \quad Y_2'(ka) \sim \frac{8}{\pi k^3 a^3} \tag{4.16}$$

are large, the coefficients B_m^Y, C_m^Y and D_m^Y will be determined by the boundary conditions on the cylinder surface. It is straightforward to verify that

$$B_m^Y = \frac{\pi}{4}\,\mathrm{e}^{\mathrm{i}mkD}(A^+ + A^-), \tag{4.17a}$$

$$C_m^Y = -\frac{\pi\mathrm{i}}{2}\,\mathrm{e}^{\mathrm{i}mkD}(A^+ - A^-), \tag{4.17b}$$

$$D_m^Y = \frac{\mu^2\pi}{16}\,\mathrm{e}^{\mathrm{i}mkD}(A^+ + A^-) = O(\mu^2). \tag{4.17c}$$

On the other hand, the coefficients B_m^J, C_m^J, D_m^J will be chosen so that the series of χ and hence $\phi_2^{(1)}$ is Bloch-periodic and bounded for large N. Details of this reasoning are lengthy and given in Appendix A. We simply cite the result, after omitting a series of $O(\mu^2)$:

$$\chi(x, y) = \frac{\pi}{4}(A^+ + A^-)\sum_{m=-N}^{N} \mathrm{e}^{\mathrm{i}mkD}(Y_0(kr_m) + J_0(kr_m))$$
$$- \frac{\pi\mathrm{i}}{2}(A^+ - A^-)\sum_{m=-N}^{N} \mathrm{e}^{\mathrm{i}mkD}(Y_1(kr_m) + J_1(kr_m))\cos\theta_m + O(\mu^2). \tag{4.18}$$

With this result, $\phi_2^{(1)}$ is known from (4.14).

4.2. *Boundary-value problem for* $\phi_2^{(2)}$

The boundary-value problem for $\phi_2^{(2)}$ is given by

$$\nabla^2\phi_2^{(2)} + \frac{\partial^2\phi_2^{(2)}}{\partial z^2} = -2\frac{\partial^2\phi_1}{\partial x\,\partial x_1} \qquad \text{in the fluid domain,} \tag{4.19}$$

$$\frac{\partial\phi_2^{(2)}}{\partial z} - \frac{\omega^2}{g}\phi_2^{(2)} = \frac{2\mathrm{i}\omega}{g}\frac{\partial\phi_1}{\partial t_1} \qquad \text{on} \quad z = 0, \tag{4.20}$$

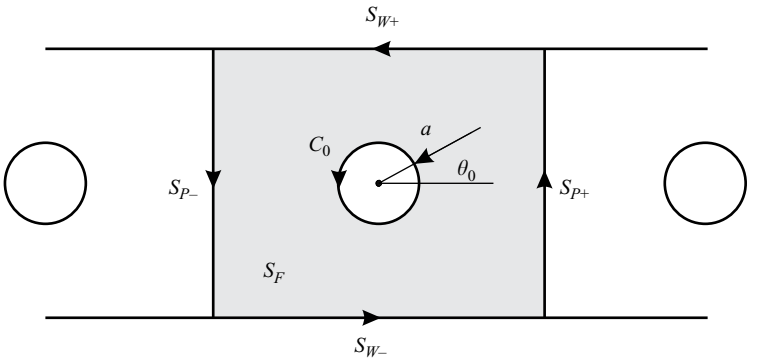

FIGURE 2. The unit cell surrounding a cylinder. C_0 is the waterline of the cylinder.

$$\frac{\partial \phi_2^{(2)}}{\partial y} = -\frac{\partial \phi_2^{(1)}}{\partial y} \qquad \text{on} \quad y = \pm\frac{W}{2}, \tag{4.21}$$

$$\frac{\partial \phi_2^{(2)}}{\partial z} = 0 \qquad \text{on} \quad z = -H. \tag{4.22}$$

On the cylinder surface, we have, by using (4.3) and (4.8),

$$\frac{\partial \phi_2^{(2)}}{\partial r_m} = -\frac{\partial \phi_2^{(1)}}{\partial r_m} - \frac{1}{\mu^2}\frac{\partial \phi_1}{\partial r_m} \qquad \text{on} \quad r_m = a. \tag{4.23}$$

Substituting (4.13) and (4.7) into (4.23), we find that the dominant part of the right-hand side of (4.23) is of order unity, i.e.

$$\frac{\partial \phi_2^{(2)}}{\partial r_m} = O(\mu^0) \qquad \text{on} \quad r_m = a. \tag{4.24}$$

Since the boundary value is effective over the small circumference $ka = O(\mu)$, its effect on $\phi_2^{(2)}$ is small. The above finite boundary value is of consequence only at the next order.

Forced by ϕ_1 and $\phi_2^{(1)}$, both of which are Bloch-periodic, $\phi_2^{(2)}$ must behave likewise, hence

$$\phi_2^{(2)}(x + D, y, z) = \mathrm{e}^{\mathrm{i}kD}\phi_2^{(2)}(x, y, z). \tag{4.25}$$

Because the inhomogeneous boundary-value problem for $\phi_2^{(2)}(x, y, z)$ has the non-trivial homogeneous solution

$$\psi^{\pm} = Z(z)\,\mathrm{e}^{\pm \mathrm{i}kx} \tag{4.26}$$

we must examine the solvability of the inhomogeneous problem in order to avoid secularity. This will yield the evolution equations for A^+ and A^-.

5. Solvability condition and wave envelope equations

Referring to figure 2, let us now define a unit cell of volume V to be the fluid region within $-D/2 \leqslant x \leqslant D/2$, $-W/2 \leqslant y \leqslant W/2$, $-H \leqslant z \leqslant 0$. Applying Green's theorem to

the homogeneous solutions $\psi^{\pm} = Z(z)\,\mathrm{e}^{\pm \mathrm{i}kx}$ and $\phi_2^{(2)}$ over V, we obtain

$$\iiint_V \left\{ \phi_2^{(2)} \left(\nabla^2 + \frac{\partial^2}{\partial z^2} \right) \psi^{\pm} - \psi^{\pm} \left(\nabla^2 + \frac{\partial^2}{\partial z^2} \right) \phi_2^{(2)} \right\} \mathrm{d}V = \iint_{\partial V} \left\{ \phi_2^{(2)} \frac{\partial \psi^{\pm}}{\partial n} - \psi^{\pm} \frac{\partial \phi_2^{(2)}}{\partial n} \right\} \mathrm{d}S. \quad (5.1)$$

The boundary surface ∂V consists of the seabed, the free surface, the periodic boundaries $S_{P\pm}$ at $x = \pm D/2$ and the sidewalls $S_{W\pm}$. Since the cylinder radius is very small, contributions from the cylinder volume or surface are negligible with error of $O(\mu^2)$. Thus, it follows from (3.8) and (4.19) that the volume integral on the left-hand side of (5.1) is

$$\begin{aligned} \mathrm{LHS}(5.1) &= 2 \iiint_V \psi^{\pm} \frac{\partial^2 \phi_1}{\partial x \partial x_1} \mathrm{d}V \\ &= 2 \int_{-H}^{0} Z^2(z)\,\mathrm{d}z \int_{-W/2}^{W/2} \mathrm{d}y \int_{-D/2}^{D/2} \mathrm{e}^{\pm \mathrm{i}kx} \left(\mathrm{i}k \frac{\partial A^+}{\partial x_1} \mathrm{e}^{\mathrm{i}kx} - \mathrm{i}k \frac{\partial A^-}{\partial x_1} \mathrm{e}^{-\mathrm{i}kx} \right) \mathrm{d}x \\ &= \mp 2\mathrm{i}kDW \frac{\partial A^{\mp}}{\partial x_1} \int_{-H}^{0} Z^2(z)\,\mathrm{d}z. \end{aligned} \quad (5.2)$$

The small area of the cylinder is ignored. The surface integral over the seabed vanishes. Using (4.20), the surface integral over the free surface is

$$\begin{aligned} \iint_{S_F} \left\{ \phi_2^{(2)} \frac{\partial \psi^{\pm}}{\partial z} - \psi^{\pm} \frac{\partial \phi_2^{(2)}}{\partial z} \right\} \mathrm{d}S &= -\frac{2\mathrm{i}\omega}{g} \iint_{S_F} \psi^{\pm} \frac{\partial \phi_1}{\partial t_1} \mathrm{d}S \\ &= -\frac{2\mathrm{i}\omega}{g} Z^2(0) \int_{-W/2}^{W/2} \mathrm{d}y \int_{-D/2}^{D/2} \mathrm{e}^{\pm \mathrm{i}kx} \left(\frac{\partial A^+}{\partial t_1} \mathrm{e}^{\mathrm{i}kx} + \frac{\partial A^-}{\partial t_1} \mathrm{e}^{-\mathrm{i}kx} \right) \mathrm{d}x \\ &= -\frac{2\mathrm{i}\omega DW}{g} Z^2(0) \frac{\partial A^{\mp}}{\partial t_1}. \end{aligned} \quad (5.3)$$

It is easy to see that the remaining integrals in (5.1) are all linear in A^+ and A^-, hence Green's formula should yield two linear partial differential equations of first order coupling $A^{\pm}$. The derivations of the remaining coefficients are provided in Appendix B; here we cite the simple results:

$$\frac{\partial A^+}{\partial t_1} + C_g \frac{\partial A^+}{\partial x_1} = -\frac{1}{2}\mathrm{i}\Omega_0(-A^+ + 3A^-), \quad (5.4a)$$

$$\frac{\partial A^-}{\partial t_1} - C_g \frac{\partial A^-}{\partial x_1} = -\frac{1}{2}\mathrm{i}\Omega_0(-A^- + 3A^+), \quad (5.4b)$$

where C_g denotes the group velocity and

$$\Omega_0 = \frac{\pi C_g}{kDW} = \frac{C_g}{n_B W} \quad (5.5)$$

is the coupling constant between the incident and reflected waves. Returning to physical coordinates according to (3.2) and using $\mu = ka$, the envelope equations† are

$$\frac{\partial A^+}{\partial t} + C_g \frac{\partial A^+}{\partial x} = -\frac{1}{2}\mathrm{i}(ka)^2 \Omega_0(-A^+ + 3A^-), \tag{5.6a}$$

$$\frac{\partial A^-}{\partial t} - C_g \frac{\partial A^-}{\partial x} = -\frac{1}{2}\mathrm{i}(ka)^2 \Omega_0(-A^- + 3A^+). \tag{5.6b}$$

The coupling of the transmitted and reflected waves is naturally stronger for larger cylinders, and for a narrower channel. In open water without cylinders, the equations for A^+ and A^- are decoupled:

$$\frac{\partial A^\pm}{\partial t_1} \pm C_g \frac{\partial A^\pm}{\partial x_1} = 0, \qquad a = 0, \tag{5.7}$$

which are well known for dispersive water waves in unobstructed sea.

We remark that when a train of water waves propagates over sinusoidal sandbars whose wavelength is half the water wavelength, the equations for the transmitted and reflected wave envelopes are similar but with differences:

$$\frac{\partial A^+}{\partial t_1} + C_g \frac{\partial A^+}{\partial x_1} = -\mathrm{i}\Omega_B A^-, \tag{5.8a}$$

$$\frac{\partial A^-}{\partial t_1} + C_g \frac{\partial A^-}{\partial x_1} = -\mathrm{i}\Omega_B A^+, \tag{5.8b}$$

where the coupling coefficient Ω_B is proportional to the bar amplitude (Mei 1985). To see the reason for this difference and for the numerical factors 1 and 3 on the right-hand sides of (5.6*a*) and (5.6*b*), we note that for sand bars of small steepness, $ka_B = O(\mu)$, the reflection coefficient of one bar is of $O(\mu)$ but the transmission coefficient is changed from unity by $O(\mu^2)$ due to energy conservation ($|R|^2 + |T|^2 = 1$). The cumulative effect of Bragg resonance is to transfer energy from waves in one direction to waves in the opposite direction. However for scattering by a single cylinder in a channel Miles (1982) has shown that

$$R = -\mu^2 \left(\frac{3\pi\mathrm{i}}{2kW}\right) + \mu^4 \left(\frac{3\pi^2}{4k^2W^2}\right) + O(\mu^6), \tag{5.9a}$$

$$T = 1 + \mu^2 \left(\frac{\pi\mathrm{i}}{2kW}\right) - \mu^4 \left(\frac{5\pi^2}{4k^2W^2}\right) + O(\mu^6), \tag{5.9b}$$

which satisfies $|R|^2 + |T|^2 = 1$ up to the accuracy of $O(\mu^8)$. Thus, both the transmitted and reflected waves are affected at the same order, $O(\mu^2)$, by scattering, and at the ratio of 3 to 1. With many cylinders Bragg resonance of waves in one direction produces comparably large cumulative effects on waves propagating in both the forward and backward directions. Thus, in (5.4*a*) for the right-going envelope A^+, the forcing comes from both the left-going wave A^- and the right-going wave A^+, with the intensity ratio of 3 to 1. Similarly, in (5.4*b*) for the left-going envelope A^-, the forcing comes from the right-going wave A^+ and the left-going wave A^-, with the same intensity ratio. Numerical confirmation of the coupled-mode equations will be given in § 9.

An immediate consequence of the envelope equations is the following energy identity. Multiplying (5.4*a*) with the complex conjugate $A^{+,*}$, and adding the result to

† Similar equations in the optics of layered media are called coupled-mode equations (Yariv & Yeh 1984).

its complex conjugate, we obtain

$$\frac{1}{2}\left(\frac{\partial|A^+|^2}{\partial t_1}+C_g\frac{\partial|A^+|^2}{\partial x_1}\right)=\frac{1}{2}\mathrm{i}\Omega_0(-3A^{+,*}A^-+3A^+A^{-,*}). \tag{5.10}$$

Applying the same procedure to (5.4*b*), we obtain

$$\frac{1}{2}\left(\frac{\partial|A^-|^2}{\partial t_1}-C_g\frac{\partial|A^-|^2}{\partial x_1}\right)=\frac{1}{2}\mathrm{i}\Omega_0(3A^{+,*}A^--3A^+A^{-,*}). \tag{5.11}$$

The sum of (5.10) and (5.11) gives the law of wave energy conservation:

$$\frac{\partial}{\partial t_1}(|A^+|^2+|A^-|^2)+C_g\frac{\partial}{\partial x_1}(|A^+|^2-|A^-|^2)=0. \tag{5.12}$$

Thus, the growth or decay of wave energy between two stations x and $x+\mathrm{d}x$ is balanced by the net influx of energy at the two ends.

We now study the physical implications of the envelope equations for several examples, restricting attention to the case $n_B=1$ or $kD=\pi$, the first Bragg resonance. For other integral values of n_B, a similar treatment can be carried out.

6. Dispersion of a transient wave packet in an infinite domain

From (5.4*a*) and (5.4*b*), $A^\pm$ can be expressed in terms of $A^\mp$:

$$A^-=\frac{2\mathrm{i}}{3\Omega_0}\left(\frac{\partial A^+}{\partial t_1}+C_g\frac{\partial A^+}{\partial x_1}-\frac{1}{2}\mathrm{i}\Omega_0A^+\right). \tag{6.1}$$

$$A^+=\frac{2\mathrm{i}}{3\Omega_0}\left(\frac{\partial A^-}{\partial t_1}-C_g\frac{\partial A^-}{\partial x_1}-\frac{1}{2}\mathrm{i}\Omega_0A^-\right). \tag{6.2}$$

Substituting (6.1) in (5.4*b*) or (6.2) in (5.4*a*), we find the governing equation for either envelope:

$$\left(\frac{\partial^2}{\partial t_1^2}-\mathrm{i}\Omega_0\frac{\partial}{\partial t_1}-C_g^2\frac{\partial^2}{\partial x_1^2}+2\Omega_0^2\right)A^\pm=0, \tag{6.3}$$

which differs from the Klein–Gordon equation by the appearance of the second term. Consider the following solutions in an infinite domain:

$$A^\pm(x_1,t_1)=A_0\,\mathrm{e}^{\pm\mathrm{i}Kx_1-\mathrm{i}\Omega t_1} \tag{6.4}$$

where μ^2K and $\mu^2\Omega$ correspond to detuning of wavenumber and frequency respectively. Equation (6.3) gives the dispersion relation:

$$K^2=\frac{\Omega^2+\Omega_0\Omega-2\Omega_0^2}{C_g^2}=\left(\frac{\Omega_0}{C_g}\right)^2\left(\frac{\Omega}{\Omega_0}+2\right)\left(\frac{\Omega}{\Omega_0}-1\right). \tag{6.5}$$

Thus for real Ω, K is complex, which is plotted in figure 3. Within the dimensionless band gap $-2<\Omega/\Omega_0<1$, the envelope wavenumber K is imaginary. Propagation is forbidden in this stopping band. Spatial attenuation is the greatest at $\Omega/\Omega_0=-1/2$. In contrast, Bragg resonance by sand bars (Mei 1985) attains its maximum spatial attenuation at perfect detuning $\Omega/\Omega_0=0$. In physical units, the band gap width is $3k^2a^2\Omega_0=3k^2a^2C_g/W$ which is inversely proportional to the channel width W. Outside the dimensionless band gap, $\Omega/\Omega_0\leqslant-2$, or $\Omega/\Omega_0\geqslant1$, K is real and the wave envelopes behave as dispersive progressive waves.

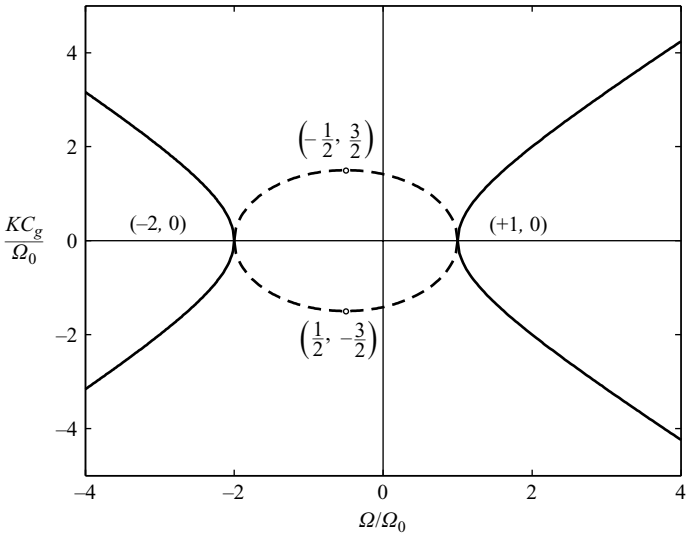

FIGURE 3. Dispersion relation of water waves through infinite periodic cylinders. Solid curve: $\mathrm{Re}(KC_g/\Omega_0)$, dashed curve: $\mathrm{Im}(KC_g/\Omega_0)$.

In order to see the physical consequence of envelope dispersion let us consider the transient evolution of a wave packet initially consisting only of right-going waves:

$$A^+(x_1,0)=\begin{cases}\frac{1}{2}(1+\cos\pi x_1/L), & |x_1|\leqslant L,\\ 0, & |x_1|>L,\end{cases}\quad\text{and}\quad A^-(x_1,0)=0,\quad -\infty<x_1<\infty. \tag{6.6}$$

Employing the exponential Fourier transform and its inverse,

$$\bar{F}(\alpha)=\int_{-\infty}^{\infty}\mathrm{e}^{-\mathrm{i}\alpha x_1}F(x_1)\,\mathrm{d}x_1,\quad F(x_1)=\frac{1}{2\pi}\int_{-\infty}^{\infty}\mathrm{e}^{\mathrm{i}\alpha x_1}\bar{F}(\alpha)\,\mathrm{d}\alpha, \tag{6.7}$$

we find the transforms of the initial envelopes

$$\bar{A}_0(\alpha)\equiv\bar{A}^+(\alpha,0)=\frac{\pi^2\sin\alpha L}{\alpha L^2(\pi^2/L^2-\alpha^2)},\quad \bar{A}^-(\alpha,0)=0. \tag{6.8}$$

The solution is

$$A^{\pm}(x_1,t_1)=\frac{1}{2\pi}\int_{-\infty}^{\infty}\mathrm{d}\alpha\,\mathscr{F}_1^{\pm}(\alpha)\,\mathrm{e}^{\mathrm{i}\alpha x_1+\mathrm{i}\sigma_1(\alpha)t_1}+\frac{1}{2\pi}\int_{-\infty}^{\infty}\mathrm{d}\alpha\mathscr{F}_2^{\pm}(\alpha)\,\mathrm{e}^{\mathrm{i}\alpha x_1+\mathrm{i}\sigma_2(\alpha)t_1}, \tag{6.9}$$

with the amplitude spectra

$$\begin{bmatrix}\mathscr{F}_1^+(\alpha)\\ \mathscr{F}_2^+(\alpha)\end{bmatrix}=\left(\frac{1}{2}\mp\frac{\alpha C_g}{\sqrt{4\alpha^2C_g^2+9\Omega_0^2}}\right)\bar{A}_0(\alpha), \tag{6.10a}$$

$$\begin{bmatrix}\mathscr{F}_1^-(\alpha)\\ \mathscr{F}_2^-(\alpha)\end{bmatrix}=\mp\frac{3\Omega_0}{2\sqrt{4\alpha^2C_g^2+9\Omega_0^2}}\bar{A}_0(\alpha), \tag{6.10b}$$

and the frequency functions

$$\begin{bmatrix}\sigma_1(\alpha)\\ \sigma_2(\alpha)\end{bmatrix} = \begin{bmatrix}\frac{1}{2}\left(\Omega_0 + \sqrt{9\Omega_0^2 + 4\alpha^2 C_g^2}\right) > 0\\ \frac{1}{2}\left(\Omega_0 - \sqrt{9\Omega_0^2 + 4\alpha^2 C_g^2}\right) < 0\end{bmatrix}, \tag{6.11}$$

which are of opposite sign. The asymptotic behaviour of the two integrals in (6.9) as seen at large t_1 by an observer travelling at some fixed speed $\xi = x_1/t_1$ can be found by the method of stationary phase.

Let the phase functions in (6.9) be defined by

$$f_1(\alpha) = \alpha\xi + \sigma_1(\alpha), \qquad f_2(\alpha) = \alpha\xi + \sigma_2(\alpha). \tag{6.12}$$

Each can have its own stationary phase point at α_1^* or α_2^* satisfying

$$-\xi = \frac{\mathrm{d}\sigma_1}{\mathrm{d}\alpha} = \frac{2\alpha_1^* C_g^2}{\sqrt{9\Omega_0^2 + 4\alpha_1^{*2} C_g^2}}, \qquad -\xi = \frac{\mathrm{d}\sigma_2}{\mathrm{d}\alpha} = \frac{-2\alpha_2^* C_g^2}{\sqrt{9\Omega_0^2 + 4\alpha_2^{*2} C_g^2}}. \tag{6.13}$$

Equations (6.13) are solved to find the points of stationary phase:

$$\alpha_1^* = -\frac{3\Omega_0\xi}{2C_g\sqrt{C_g^2 - \xi^2}}, \qquad \alpha_2^* = \frac{3\Omega_0\xi}{2C_g\sqrt{C_g^2 - \xi^2}}, \tag{6.14}$$

which exist only when $-C_g < \xi < C_g$. Physically, $\mu^2\alpha_1^*$ and $\mu^2\alpha_2^*$ are the wavenumbers of sinusoidal envelope waves.

By the standard theory of stationary phase, the large-time approximation of (6.9) is

$$A^{\pm}(x_1, t_1) \approx \frac{\mathscr{F}_1^{\pm}(\alpha_1^*)\,\mathrm{e}^{\mathrm{i}(\alpha_1^* x_1 + \sigma_1(\alpha_1^*)t_1 + \pi/4)}}{\sqrt{2\pi\sigma_1''(\alpha_1^*)t_1}} + \frac{\mathscr{F}_2^{\pm}(\alpha_2^*)\,\mathrm{e}^{\mathrm{i}(\alpha_2^* x_1 + \sigma_2(\alpha_2^*)t_1 + \pi/4)}}{\sqrt{2\pi\sigma_2''(\alpha_1^*)t_1}}, \tag{6.15}$$

where

$$\begin{bmatrix}\sigma_1''(\alpha_1^*)\\ \sigma_2''(\alpha_2^*)\end{bmatrix} = \frac{2\left(C_g^2 - \xi^2\right)^{3/2}}{3\Omega_0 C_g} > 0. \tag{6.16}$$

Thus a moving observer sees two sinusoidal envelope waves with amplitudes decaying in time as $t_1^{1/2}$. At any fixed t_1, the envelope-wave amplitude is the largest, while its wavelength is the shortest, near the front. The reverse is true near the origin. At the front the approximation breaks down. A better approximation is possible but not pursued here (see e.g. Kajiura 1963 or Mei 1989 for an open sea).

To an observer travelling to the right at a fixed speed lower than the group speed of the carrier wave, $0 < \xi < C_g$, two sinusoidal envelope waves are seen. Since $(\alpha_1^* < 0, \sigma_1(\alpha_1^*) > 0)$ and $(\alpha_2^* > 0, \sigma_2(\alpha_2^*) < 0)$, both envelope waves propagate rightward (away from the origin). Since $|\alpha_1^*| = |\alpha_2^*|$ and $\sigma_1(\alpha_1^*) > \sigma_2(\alpha_2^*)$, both envelope waves have the same local wavelength but different frequencies, corresponding to the two branches of the dispersion diagram in figure 3. The first (with subscript 1) advances faster than the second. Within each envelope wave there are monochromatic and progressive carrier waves of frequency ω and wavenumber k propagating in two opposite directions. The local amplitudes of these opposing carrier waves are different. For example, in the faster envelope wave, the right-going and left-going carrier waves

have the amplitude ratio

$$\frac{|\mathscr{F}_1^+(\alpha_1^*)|}{|\mathscr{F}_1^-(\alpha_1^*)|} = \frac{\sqrt{\alpha_1^{*2}C_g^2 + \frac{9}{4}\Omega_0^2} + |\alpha_1^*|C_g}{\frac{3}{2}\Omega_0} > 1, \tag{6.17}$$

hence their sum constitutes a partially standing carrier wave. Standing carrier waves with the same amplitude ratio reside in the slower envelope wave since $\alpha_2^* = |\alpha_1^*|$.

Similarly, two sinusoidal envelope waves are also seen by an observer travelling to the left at a speed lower than the group speed of the carrier wave, $-C_g < \xi < 0$. Since $(\alpha_1^* > 0, \sigma_1(\alpha_1^*) > 0)$ and $(\alpha_2^* < 0, \sigma_2(\alpha_2^*) < 0)$, both envelope waves propagate leftward. Again in each envelope wave the opposing carrier waves form a partially standing wave.

Also, in view of (6.8), the wave envelopes have moving nodes at

$$\sin \alpha_{1,2}^* L = 0 \tag{6.18}$$

which occur at

$$\frac{3\Omega_0 \xi L}{2C_g\sqrt{C_g^2 - \xi^2}} = n\pi, \qquad n = 0, 1, \ldots. \tag{6.19}$$

Thus the nodes move to the right at the constant speed of

$$\xi = \frac{x_1}{t_1} = \pm\frac{C_g}{[1 + (3\Omega_0 L/(2n\pi C_g))^2]^{1/2}}, \qquad n = 0, 1, \ldots. \tag{6.20}$$

At these nodes, the observer sees no wave.

7. A semi-infinite line of cylinders and wave trapping

We consider next the Bragg scattering of water waves by a semi-infinite line of periodic cylinders covering the range $0 < x_1 < \infty$. Let the rightward incident wave and the leftward reflected wave be

$$A^+(x_1, t_1) = A_0 T(x_1)\, \mathrm{e}^{-\mathrm{i}\Omega t_1}, \quad A^-(x_1, t_1) = A_0 R(x_1)\, \mathrm{e}^{-\mathrm{i}\Omega t_1}, \quad x_1 > 0, \tag{7.1}$$

where T and R represent local transmission and reflection coefficients respectively. It is easy to show that

$$T = \mathrm{e}^{-Q\Omega_0 x_1/C_g}, \quad R(x_1) = R(0)\, \mathrm{e}^{-Q\Omega_0 x_1/C_g} \tag{7.2}$$

where

$$Q = \sqrt{\left(\frac{\Omega}{\Omega_0} + 2\right)\left(1 - \frac{\Omega}{\Omega_0}\right)}. \tag{7.3}$$

Within the band gap $-2 < \Omega/\Omega_0 < 1$, Q is real, hence waves are localized within the dimensionless distance $C_g/\Omega_0 Q$. In particular the reflection coefficient at the entrance $x_1 = 0$ is

$$R(0) = \frac{3}{1 + 2(\Omega/\Omega_0) + 2\mathrm{i}Q} = \mathrm{e}^{\mathrm{i}\Theta}, \tag{7.4}$$

Reflection is perfect with the phase change

$$\Theta = \arg\left(1 + \frac{2\Omega}{\Omega_0} - 2\mathrm{i}Q\right). \tag{7.5}$$

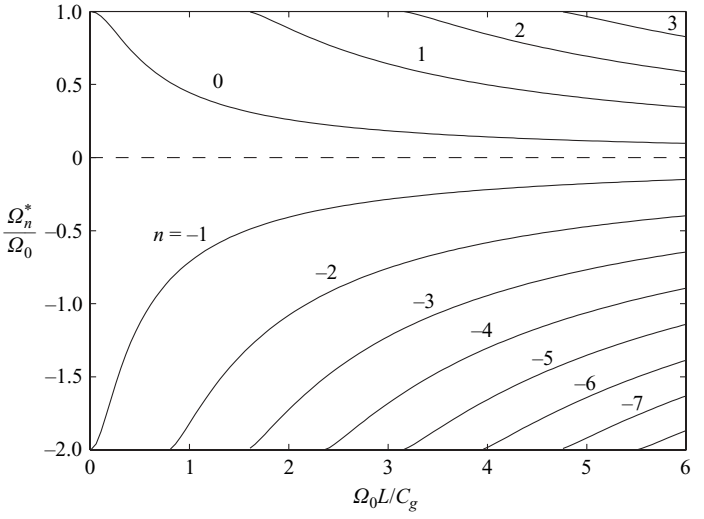

FIGURE 4. Natural detuned frequencies of trapped envelopes Ω_n^*/Ω_0 against $\Omega_0 L/C_g$, the dimensionless width of an open strip sandwiched between two long strips of cylinders.

Similarly if the cylinders are distributed instead on the left, $-\infty < x_1 < 0$, and a leftward incident wavetrain arrives from $x_1 > 0$, the envelopes of right- and left-going waves in the region $x_1 < 0$ are respectively

$$B^+ = B_0 R(0)\, \mathrm{e}^{\Omega_0 C_g x_1/Q}\, \mathrm{e}^{-\mathrm{i}\Omega t_1}, \qquad B^- = B_0\, \mathrm{e}^{\Omega_0 C_g x_1/Q}\, \mathrm{e}^{-\mathrm{i}\Omega t_1}. \tag{7.6}$$

Let us now consider a strip $-L < x_1 < L$ of open water (cylinder-free) sandwiched by two semi-infinite domains of cylinders. The envelopes of right- and left-going waves are respectively $C\,\mathrm{e}^{\mathrm{i}Kx_1}$ and $D\,\mathrm{e}^{-\mathrm{i}Kx_1}$, where $K = \Omega/C_g$. Changing x_1 to $x_1 - L$ in (7.1) and to $x_1 + L$ in (7.6), then matching at the junctions $x_1 = -L$ and $x_1 = L$, obtain

$$B_0 R(0) = C\,\mathrm{e}^{-\mathrm{i}KL}, \quad B_0 = D\,\mathrm{e}^{\mathrm{i}KL}, \quad C\,\mathrm{e}^{\mathrm{i}KL} = A_0, \quad D\,\mathrm{e}^{-\mathrm{i}KL} = A_0 R(0). \tag{7.7}$$

This is a set of homogeneous equations for the coefficients A_0, B_0, C and D. Non-trivial solution requires that

$$\sin(2KL + \Theta) = 0 \tag{7.8}$$

which is the eigenvalue condition for Ω. Using (7.5) the natural detuning frequencies Ω_n^* of the wave envelope are given implicitly by

$$2\frac{\Omega_0 L}{C_g}\frac{\Omega_n^*}{\Omega_0} + \Theta = n\pi, \qquad n = 0, \pm 1, \ldots. \tag{7.9}$$

At each eigenfrequency Ω_n^*, the wave envelopes are trapped in the centre strip.

Real solutions of (7.9) lie within the range $-2 < \Omega_n^*/\Omega_0 < 1$, which indicates that trapped modes are present only when the detuning frequency lies within the band gap.

Figure 4 shows the dependence of non-dimensional eigenfrequencies Ω_n^*/Ω_0 on the dimensionless centre strip length $\Omega_0 L/C_g$. It can be seen that the number of trapped modes increases with the strip length for different n.

8. Scattering by a finite strip of periodic cylinders

8.1. *Governing equations and boundary conditions*

As another application, we consider a large but finite number of periodic cylinders in the strip $0 \leqslant x_1 \leqslant L$, bounded by open waters outside. The incident wavetrain arrives from $x \sim -\infty$ with the wavenumber $k + \mu^2 K$ slightly detuned from Bragg resonance. The corresponding frequency is shifted by the amount $\mu^2 \Omega = \mu^2 C_g K$, where K and Ω are of order unity,

$$A^+(x_1, t_1) = A_0 \mathrm{e}^{\mathrm{i}(K x_1 - \Omega t_1)}. \tag{8.1}$$

In the cylinder region, we assume the envelopes to be of the form

$$A^+(x_1, t_1) = A_0 T(x_1)\, \mathrm{e}^{-\mathrm{i}\Omega t_1}, \quad A^-(x_1, t_1) = A_0 R(x_1)\, \mathrm{e}^{-\mathrm{i}\Omega t_1}, \tag{8.2}$$

where $T(x_1)$ and $R(x_1)$ are the local transmission and reflection coefficients, respectively. It follows readily from the evolution equation (6.3) that

$$\frac{\mathrm{d}^2}{\mathrm{d}x_1^2}\begin{pmatrix} T \\ R \end{pmatrix} + \frac{\Omega_0^2}{C_g^2}\left(\frac{\Omega}{\Omega_0} + 2\right)\left(\frac{\Omega}{\Omega_0} - 1\right)\begin{pmatrix} T \\ R \end{pmatrix} = 0. \tag{8.3}$$

It is evident that both $T(x_1)$ and $R(x_1)$ are oscillatory in x_1 if Ω/Ω_0 lies outside the band gap and monotonic within. From (6.1) we also find

$$R = \frac{2}{3}\left(\frac{\Omega}{\Omega_0} + \frac{1}{2}\right) T + \frac{2\mathrm{i}C_g}{3\Omega_0}\frac{\mathrm{d}T}{\mathrm{d}x_1}. \tag{8.4}$$

Clearly $T(0) = 1$ at the entrance and $R(L) = 0$ at the exit. Substituting (8.2) into the energy conservation equation (5.12), we obtain after integration

$$|T(x_1)|^2 - |R(x_1)|^2 = 1 - |R(0)|^2 = |T(L)|^2, \tag{8.5}$$

or $|R(0)|^2 + |T(L)|^2 = 1$.

The solution of the boundary value problem is straightforward. We only examine the results in various parts of the frequency band.

8.2. *Outside the band gap*

Let the detuning frequency be in the range either $\Omega/\Omega_0 < -2$ or $\Omega/\Omega_0 > 1$. The solution for any x_1 in the strip is

$$T(x_1) = \frac{-[1 + 2(\Omega/\Omega_0)]\sin[[P\Omega_0 L/C_g](x_1/L - 1)] + 2\mathrm{i}P\cos[[P\Omega_0 L/C_g](x_1/L - 1)]}{[1 + 2(\Omega/\Omega_0)]\sin[P\Omega_0 L/C_g] + 2\mathrm{i}P\cos[P\Omega_0 L/C_g]}, \tag{8.6a}$$

$$R(x_1) = \frac{-3\sin[[P\Omega_0 L/C_g](x_1/L - 1)]}{[1 + 2(\Omega/\Omega_0)]\sin[P\Omega_0 L/C_g] + 2\mathrm{i}P\cos[P\Omega_0 L/C_g]}, \tag{8.6b}$$

where

$$P = \sqrt{(\Omega/\Omega_0 + 2)(\Omega/\Omega_0 - 1)} \tag{8.7}$$

is real. The scattering coefficients depend also on the dimensionless width of the strip $\Omega_0 L/C_g$.

In particular, the transmission coefficient at the exit is

$$T(L) = \frac{2\mathrm{i}P}{[1 + 2(\Omega/\Omega_0)]\sin[P\Omega_0 L/C_g] + 2\mathrm{i}P\cos[P\Omega_0 L/C_g]}, \tag{8.8}$$

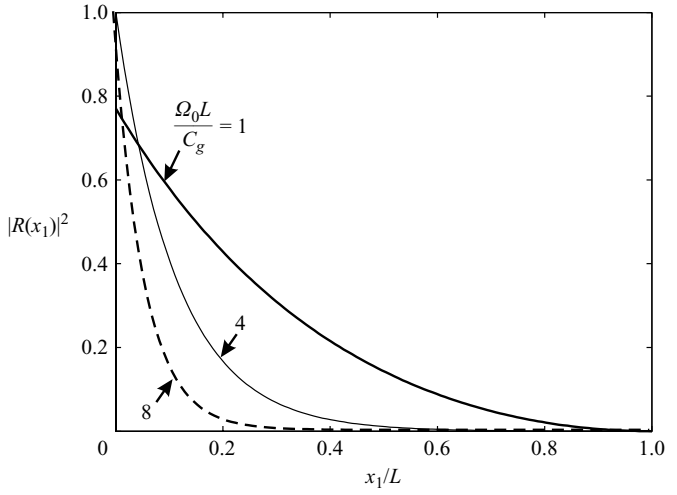

FIGURE 5. Reflection intensity along the array for various $\Omega_0 L/C_g$ with detuning parameter $\Omega/\Omega_0 = 0.5$. Thick solid curve: $\Omega_0 L/C_g = 1$, thin solid curve: $\Omega_0 L/C_g = 4$, dashed curve: $\Omega_0 L/C_g = 8$.

and the reflection coefficient at the entrance is

$$R(0) = \frac{3\sin(P\Omega_0 L/C_g)}{[1+2(\Omega/\Omega_0)]\sin[P\Omega_0 L/C_g] + 2\mathrm{i}P\cos[P\Omega_0 L/C_g]}. \tag{8.9}$$

8.3. *Within the band gap* $-2 < \Omega/\Omega_0 < 1$

The parameter P in (8.7) is purely imaginary. Let $P = \mathrm{i}Q$, where

$$Q = -\mathrm{i}P = \sqrt{(\Omega/\Omega_0 + 2)(1 - \Omega/\Omega_0)} \tag{8.10}$$

is real. We find from (8.6*a*) and (8.6*b*)

$$T(x_1) = \frac{-[1+2(\Omega/\Omega_0)]\sinh[[Q\Omega_0 L/C_g](x_1/L-1)] + 2\mathrm{i}Q\cosh[[Q\Omega_0 L/C_g](x_1/L-1)]}{[1+2(\Omega/\Omega_0)]\sinh[Q\Omega_0 L/C_g] + 2\mathrm{i}Q\cosh[Q\Omega_0 L/C_g]}, \tag{8.11a}$$

$$R(x_1) = \frac{-3\sinh[[Q\Omega_0 L/C_g](x_1/L-1)]}{[1+2(\Omega/\Omega_0)]\sinh[Q\Omega_0 L/C_g] + 2\mathrm{i}Q\cosh[Q\Omega_0 L/C_g]}. \tag{8.11b}$$

The transmission coefficient at the exit is

$$T(L) = \frac{2\mathrm{i}Q}{[1+2(\Omega/\Omega_0)]\sinh[Q\Omega_0 L/C_g] + 2\mathrm{i}Q\cosh[Q\Omega_0 L/C_g]}, \tag{8.12}$$

and the reflection coefficient at the entrance is

$$R(0) = \frac{3\sinh[Q\Omega_0 L/C_g]}{[1+2(\Omega/\Omega_0)]\sinh[Q\Omega_0 L/C_g] + 2\mathrm{i}Q\cosh[Q\Omega_0 L/C_g]}. \tag{8.13}$$

From (8.7) and (8.10), one can easily verify that, for any two incident waves with detuning frequencies Ω and Ω' which are mirror images of each other with respect to the centre of the band gap, i.e. $(\Omega + \Omega')/\Omega_0 = -1/2$, their spatial distributions of $|R(x_1)|$ and $|T(x_1)|$ are identical. Thus we only present results for $\Omega/\Omega_0 \geqslant -1/2$.

Figure 5 shows the spatial variation of the reflection coefficient $|R(x_1)|^2$ for $\Omega/\Omega_0 = 1/2$ as a function of the dimensionless width of the cylinder strip $\Omega_0 L/C_g$. The

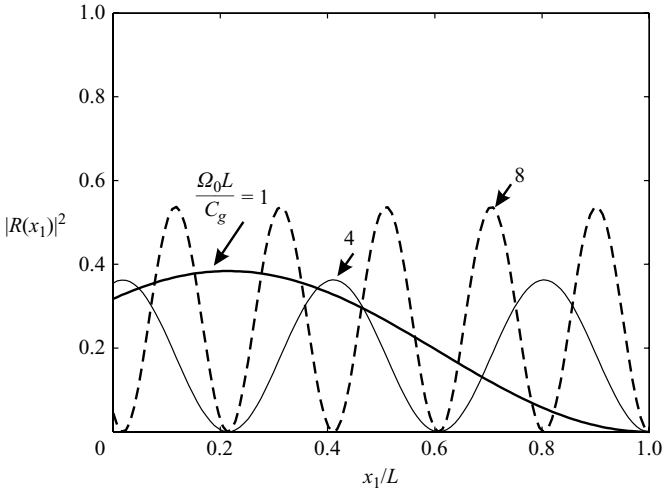

FIGURE 6. Reflection intensity along the array for various $\Omega_0 L/C_g$ with detuning parameter $\Omega/\Omega_0 = 2.0$. Thick solid curve: $\Omega_0 L/C_g = 1$, thin solid curve: $\Omega_0 L/C_g = 4$, dashed curve: $\Omega_0 L/C_g = 8$.

results are typical of all cases within the band gap, i.e. $|R(x_1)|^2$ decreases monotonically with the distance x_1 from the entrance. As L increases, the reflection coefficient at the entrance $R(0)$ approaches unity, implying complete reflection.

In figure 6, we display the reflected energy intensity $|R(x_1)|^2$ for $\Omega/\Omega_0 = 2.0$. The oscillatory feature is representative of all cases outside the band gap. Local reflection vanishes at

$$x_1 = L + \frac{m\pi C_g}{P\Omega_0}, \qquad m = -\left[\frac{P\Omega_0 L}{\pi C_g}\right], \ldots, -1, 0, \tag{8.14}$$

where the square bracket $[P\Omega_0 L/\pi C_g]$ represents the largest integer less than $P\Omega_0 L/\pi C_g$.

In figure 7, the reflection coefficient at the entrance is plotted against the detuning parameter Ω/Ω_0 for various dimensionless strip lengths $\Omega_0 L/C_g$. When $-2 \leqslant \Omega/\Omega_0 \leqslant 1$ within the band gap, reflection increases monotonically and approaches unity as the strip length increases. When the detuning Ω/Ω_0 is outside the band gap, $|R(0)|^2$ is oscillatory with respect to $\Omega_0 L/C_g$. From (8.9), zero reflection or perfect transmission is reached at $P\Omega_0 L/C_g = m\pi$ where m is any integer. Reflection diminishes as the detuning frequency increases.

For a fixed strip lengths $\Omega_0 L/C_g$, the dependence of the reflection coefficient on the detuning frequency is illustrated in figure 8. Within the band gap $-2 \leqslant \Omega/\Omega_0 \leqslant 1$ (only the upper half $-1/2 \leqslant \Omega/\Omega_0 \leqslant 1$ is shown), $|R(0)|^2$ decreases monotonically as Ω/Ω_0 increases. The reflection coefficient approaches unity quickly with increasing strip length. Outside the band gap, $\Omega/\Omega_0 > 2$, $|R(0)|^2$ is oscillatory and in general decreases with increasing Ω/Ω_0, which can be a result of a wider channel. It can be derived from (8.7) and (8.9) that no wave is reflected by the strip when

$$\Omega/\Omega_0 = -\frac{1}{2} \pm \sqrt{\frac{m\pi}{\Omega_0 L/C_g} + \frac{9}{4}}, \quad m \text{ is any integer} \geqslant -\frac{9\Omega_0 L/C_g}{4\pi}. \tag{8.15}$$

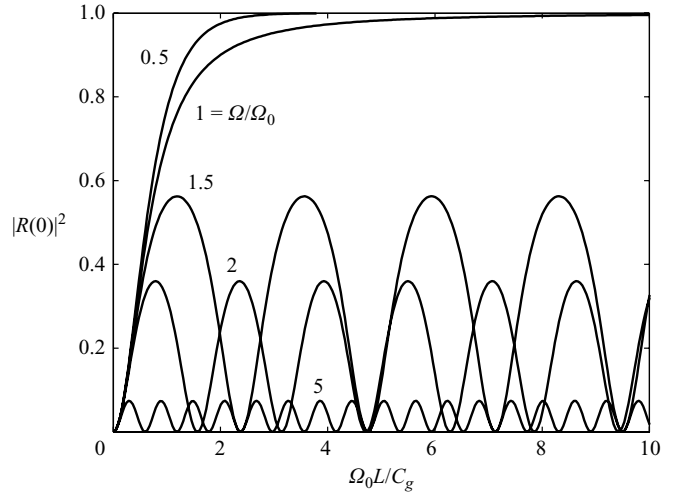

FIGURE 7. Dependence of the reflection intensity at inlet $x_1 = 0$ on strip length $\Omega_0 L/C_g$ for various detuning parameter values $\Omega/\Omega_0 = 0.5, 1.0, 1.5, 2.0, 5$.

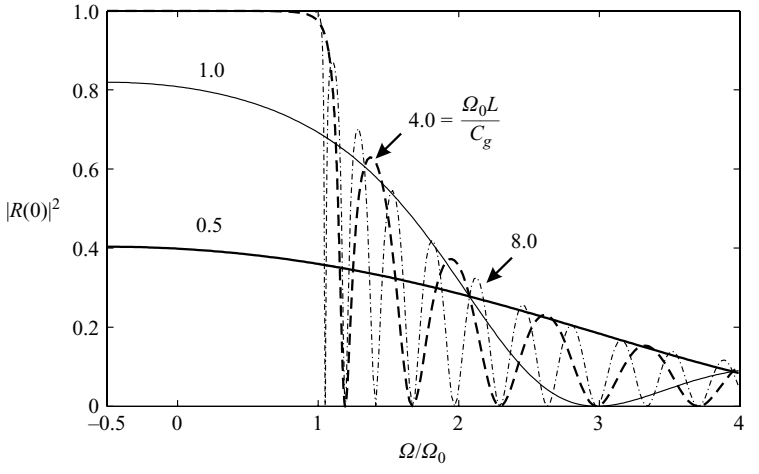

FIGURE 8. Dependence of the reflection intensity at $x_1 = 0$ on detuning parameter Ω/Ω_0 for various strip length values $\Omega_0 L/C_g = 0.5, 1.0, 4.0, 8.0$.

From (8.9), the oscillation of $|R(0)|^2$ with respect to Ω becomes faster for a longer strip.

9. Comparison with numerical solution by finite elements

In order to see the range of validity of the asymptotic theory we have carried out direct numerical computation for the linear wave scattering problem around a large but finite number of circular cylinders in a channel. The hybrid finite element method developed by earlier authors (Bai & Yeung 1974; Chen & Mei 1974*a*,*b*; Yue, Chen & Mei 1978; Li & Mei 2006) was used. In that method, which is applicable in principle for scatterers of arbitrary size and geometry, the fluid domain is first divided into the near field enclosing all the scatterers, and the far field of open

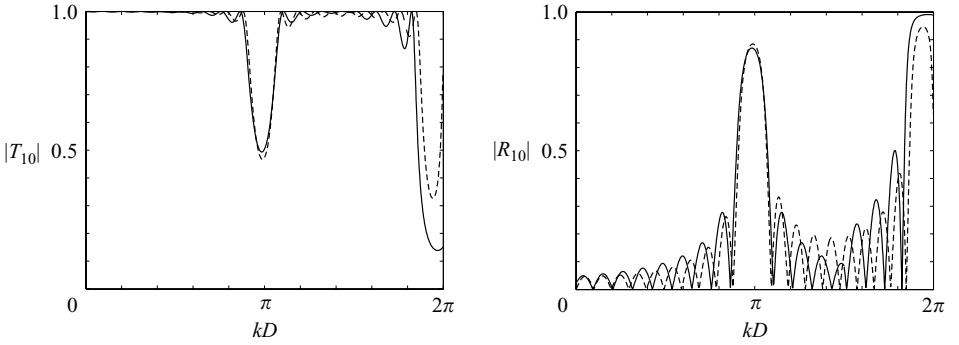

FIGURE 9. Transmission and reflection coefficients for a row of 21 ($N = 10$) circular cylinders of radius $a/D = 0.10$, $D/W = 1$. Solid curve: asymptotic solution; dashed curve: finite element solution.

waters. The velocity potential in the near field is discretized by finite elements, while the far field is represented by analytical solutions such as eigenfunction expansions. A variational principle is derived to replace the boundary value problem and the matching conditions. Extremization with respect to all unknown nodal and expansion coefficients leads to a matrix equation which is then solved numerically.

We shall only display a few sample comparisons here; more extensive comparisons have been documented in Li (2006). Results have been obtained by the hybrid element method for $0 < kD < 2\pi$ which includes the entire neighbourhood of the first Bragg resonance peak $kD = \pi$ and part of the second peak at $kD = 2\pi$. For 21 cylinders ($N = 10$) numerical simulations have been carried out for $a/D = 0.10, 0.15$. For comparison, results from the analytical formulae are obtained for the neighbourhoods of $kD = \pi$ and $kD = 2\pi$ separately. Specifically, for wavenumbers $kD \in [0, 3\pi/2]$ (around the first peak), we apply the asymptotic theory for the detuning wavenumber

$$KD = \frac{kD - k_1 D}{\mu^2} = \frac{kD - k_1 D}{(k_1 a)^2} = \frac{(kD - \pi)}{\pi^2 (a/D)^2}.$$

For wavenumbers in $kD \in [3\pi/2, 2\pi]$ (around the second peak), the theory is applied for the detuning wavenumber

$$KD = \frac{kD - k_2 D}{\mu^2} = \frac{kD - k_2 D}{(k_2 a)^2} = \frac{(kD - 2\pi)}{4\pi^2 (a/D)^2}.$$

Figures 9 and 10 are two sample comparisons for the transmission coefficient at the exit and the reflection coefficient at the entrance. For $a/D = 0.10$, the detuning frequency range is $KD \in [-100/\pi, 50/\pi]$ near the first resonance and $KD \in [-25/2\pi, 0]$ near the second resonance. For $a/D = 0.15$, the corresponding detunings are $KD \in [-400/9\pi, 200/9\pi]$ and $[-50/9\pi, 0]$ respectively. It can be seen that for sufficiently small cylinders, the asymptotic theory predicts very well the location and magnitude of the reflection and transmission coefficients at and around the first peak of Bragg resonance at $kD = \pi$ for both $a/D = 0.1$ and 0.15. The agreement near the second peak is less satisfactory and deteriorates as a/D increases. This is understandable since for the larger cylinder $a/D = 0.15$, $\mu^2 = (\pi a/D)^2 = 0.222$ at the first peak but $\mu^2 = (2\pi a/D)^2 = 0.888$ at the second peak, which is not small.

In figure 11 we increase the number of cylinders to 41 ($N = 20$) for the smaller ratio $a/D = 0.10$ with $D/W = 1$. Note first that with more cylinders reflection is greatly enhanced and transmission reduced near both peaks. The quantitative agreement with

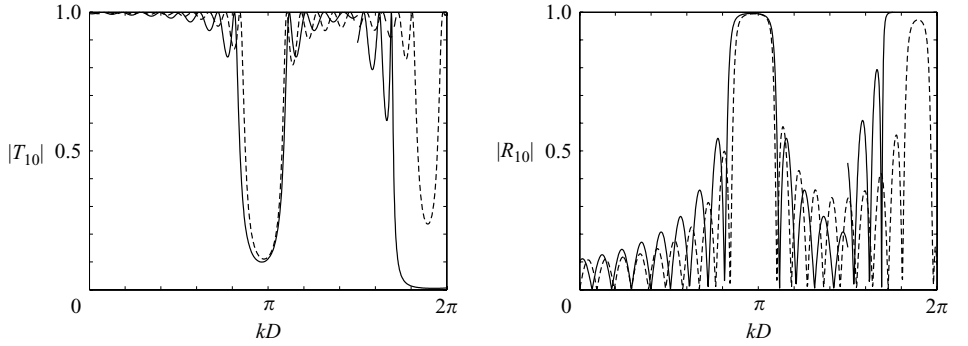

FIGURE 10. As figure 9 but for $a/D = 0.15$.

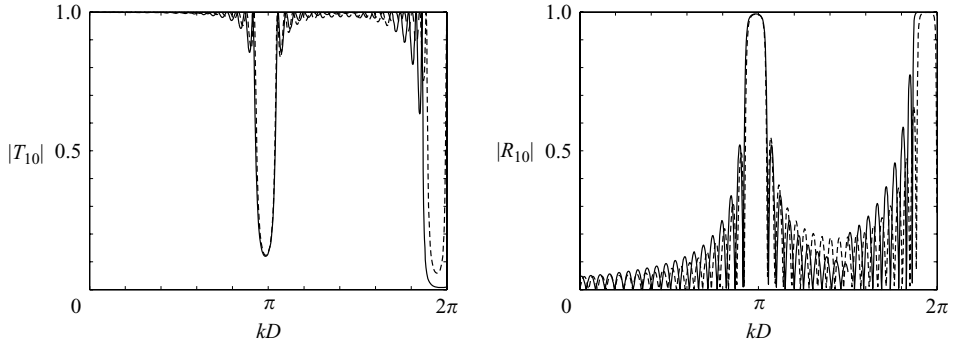

FIGURE 11. As figure 9 but for a row of 41 ($N = 20$) circular cylinders of radius $a/D = 0.10$, $D/W = 1$. Solid curve: asymptotic solution; dashed curve: finite element solution.

numerical computations is excellent due to the smallness of $\mu^2 = 0.0987$ at the first peak and $\mu^2 = 0.3948$ at the second peak.

10. Summary remarks

We have developed an asymptotic theory for the scattering of infinitesimal water waves by a long array of cylinders in a channel. This is an extension of earlier works where the geometries were strictly one-dimensional. Combining Bloch's theorem with the multiple-scale approximation, envelope equations (also called coupled mode equations in optics (Yariv & Yeh 1984)) are derived for the long-scale variations. Analytical solutions for both transient and quasi-steady incident waves are obtained and the accuracy is confirmed by direct numerical simulation. It is worth pointing that the asymptotic theory not only enhances physical discussions, but also remains computationally efficient as the number of scatterers increases. These advantages are not shared by the more numerical methods. For ocean engineering applications, the effects of vortex shedding around small cylinders must of course be accounted for in the future, not only for better modelling of the wave forces but for the variation of wave amplitudes in the region of scatterers. For two-dimensional scattering of sound by parallel cylinders, vortex shedding is unlikely to be important, and the present theory can be applied with greater assurance.

Extensions to second-order nonlinear effects and to two-dimensional arrays will be reported elsewhere.

Dedicated to the memory of Professor Howell Peregrine. We acknowledge with gratitude the financial support by US Navy, Office of Naval Research (Grant N00014-04-1-0077), US National Science Foundation (Grant CTS 007573) and US–Israel Binational Science Foundation. Discussions with Professor Jian Zi, Department of Physics, Fudan University, Shanghai, China, partly stimulated the present study.

Appendix A. Bloch's condition and the solution for χ

In order to satisfy Bloch's condition, we need to ensure that the product $e^{\pm ikx}\phi_2^{(1)} = e^{\pm ikx}\chi(x, y)Z(z)$ is periodic in x with period D. Since $e^{\pm ikx} = e^{\mp ikD}\, e^{\pm ik(x+D)}$ and $e^{ikD} = e^{in_B\pi} = e^{-ikD}$, $\chi(x, y)$ must have the following translational property:

$$\chi(x + D, y, z; x_1, t_1) = e^{ikD}\chi(x, y, z; x_1, t_1). \tag{A 1}$$

Note that r_m and θ_m depend on x such that

$$r_m(x) = \sqrt{(x - x_m^o)^2 + y^2} = \sqrt{(x + \pi/k - x_{m+1}^o)^2 + y^2} = r_{m+1}(x + \pi/k),$$
$$\theta_m(x) = \tan^{-1}\frac{x - x_m^o}{y} = \tan^{-1}\frac{x + \pi/k - x_{m+1}^o}{y} = \theta_{m+1}(x + \pi/k).$$

It follows that

$$\begin{aligned}
&\chi\left(x + D, y, z\right)\\
&= \sum_{m=-N}^{N} \left\{ \left[B_m^Y Y_0(kr_m) + B_m^J J_0(kr_m)\right] + \left[C_m^Y Y_1(kr_m) + C_m^J J_1(kr_m)\right]\cos\theta_m \right.\\
&\quad \left. + \left[D_m^Y Y_2(kr_m) + D_m^J J_2(kr_m)\right]\cos 2\theta_m \right\}_{x+D}\\
&= \sum_{m=-N}^{N} \left\{ \left[B_m^Y Y_0(kr_{m-1}) + B_m^J J_0(kr_{m-1})\right] + \left[C_m^Y Y_1(kr_{m-1}) + C_m^J J_1(kr_{m-1})\right]\cos\theta_{m-1} \right.\\
&\quad \left. + \left[D_m^Y Y_2(kr_{m-1}) + D_m^J J_2(kr_{m-1})\right]\cos 2\theta_{m-1} \right\}_{x}\\
&= \sum_{m=-N+1}^{N+1} \left\{ \left[B_{m+1}^Y Y_0(kr_m) + B_{m+1}^J J_0(kr_m)\right] + \left[C_{m+1}^Y Y_1(kr_m) + C_{m+1}^J J_1(kr_m)\right]\cos\theta_m \right.\\
&\quad \left. + \left[D_{m+1}^Y Y_2(kr_m) + D_{m+1}^J J_2(kr_m)\right]\cos 2\theta_m \right\}_{x},
\end{aligned} \tag{A 2}$$

where use is made of the fact that $N = O(\mu^{-2})$ and that the effect of shifting the whole cylinder array to the right or left by a distance of D introduces a negligible difference of $O(\mu^2)$ to the series. Substituting (A 2) into (A 1) and comparing the resulting equation with (4.15), we find

$$B_{m+1}^Y = e^{ikD}B_m^Y, \qquad C_{m+1}^Y = e^{ikD}C_m^Y, \qquad D_{m+1}^Y = e^{ikD}D_m^Y, \tag{A 3a}$$
$$B_{m+1}^J = e^{ikD}B_m^J, \qquad C_{m+1}^J = e^{ikD}C_m^J, \qquad D_{m+1}^J = e^{ikD}D_m^J. \tag{A 3b}$$

The relations (A 3a) are satisfied by (4.17a, b, c).

Using (A 3), we can write (4.15) as

$$\chi = \sum_{m=-N}^{N} \left[B_0^Y Y_0(kr_m) + B_0^J J_0(kr_m)\right] \mathrm{e}^{\mathrm{i}mkD} + \sum_{m=-N}^{N} \left[C_0^Y Y_1(kr_m) + C_1^J J_1(kr_m)\right] \mathrm{e}^{\mathrm{i}mkD} \cos\theta_m + \sum_{m=-N}^{N} \left[D_0^Y Y_2(kr_m) + D_1^J J_2(kr_m)\right] \mathrm{e}^{\mathrm{i}mkD} \cos 2\theta_m. \tag{A 4}$$

Let us first investigate the boundedness of the first series on the right-hand side of (A 4). For large $|m|$ and fixed x, $kr_m \approx |m|kD \gg 1$. The asymptotic approximation of Y_0 and J_0 for large arguments gives (see equations 9.2.1 and 9.2.2 in Abramowitz & Stegun 1972),

$$Y_0(kr_m) \approx Y_0(|m|kD) = \sqrt{\frac{2}{|m|\pi kD}} \sin\left(|m|kD - \frac{\pi}{4}\right) + O\left(\frac{1}{|m|^{3/2}}\right) = -\frac{\cos mkD}{\sqrt{|m|\pi kD}} + O\left(\frac{1}{|m|^{3/2}}\right), \tag{A 5a}$$

$$J_0(kr_m) \approx J_0(|m|kD) = \sqrt{\frac{2}{|m|\pi kD}} \cos\left(|m|kD - \frac{\pi}{4}\right) + O\left(\frac{1}{|m|^{3/2}}\right) = \frac{\cos mkD}{\sqrt{|m|\pi kD}} + O\left(\frac{1}{|m|^{3/2}}\right), \tag{A 5b}$$

because $kD = n_B\pi$. Since $\mathrm{e}^{\mathrm{i}mkD} = \cos mkD = (-1)^{mn_B}$, it follows that the mth term in the first series of (A 4) approaches, for large $|m|$,

$$\left(-B_0^Y + B_0^J\right)\left[\frac{\cos mkD}{\sqrt{|m|\pi kD}} + O\left(\frac{1}{|m|^{3/2}}\right)\right]\mathrm{e}^{\mathrm{i}mkD} = \frac{\left(-B_0^Y + B_0^J\right)}{\sqrt{|m|\pi kD}} + O\left(\frac{1}{|m|^{3/2}}\right).$$

To ensure that the first series in (A 4) is bounded as $N \to \infty$ we can only choose $B_0^J = B_0^Y$, which implies, in view of (A 3*a*, *b*),

$$B_m^J = B_m^Y = \mathrm{e}^{\mathrm{i}mkD} B_0^Y. \tag{A 6}$$

Similar analysis for the remaining two sums in (A 4) shows that

$$C_m^J = C_m^Y, \qquad D_m^J = D_m^Y = O(\mu^2). \tag{A 7}$$

With these choices, (4.15) reduces to (4.18), after omitting terms of $O(\mu^2)$.

Appendix B. Coefficients of the envelope equations

Referring to figure 2, on the end surfaces of the cell $S_{P\pm}: x = \pm\frac{1}{2}D$, $|y| \leqslant \frac{1}{2}W$, $-H \leqslant z \leqslant 0$, both $\psi^{\pm}$ and $\phi_2^{(2)}$ and their x derivatives have identical magnitudes but opposite signs. Hence the surface integral vanishes,

$$\iint_{S_P} \left\{\phi_2^{(2)} \frac{\partial \psi^{\pm}}{\partial n} - \psi^{\pm} \frac{\partial \phi_2^{(2)}}{\partial n}\right\} \mathrm{d}S = 0. \tag{B 1}$$

Care must be taken for the surface integral over the channel sidewalls $S_{W\pm}: y = \pm\frac{1}{2}W$, $|x| \leqslant \frac{1}{2}D$, $-H \leqslant z \leqslant 0$. Since the normal gradient of $\psi^{\pm}$ vanishes, it follows from (4.21) and (4.14) that the channel-wall integral reduces to

$$\iint_{S_W} \left\{ \phi_2^{(2)} \frac{\partial \psi^{\pm}}{\partial n} - \psi^{\pm} \frac{\partial \phi_2^{(2)}}{\partial n} \right\} \mathrm{d}S = \int_{-H}^{0} Z^2(z)\,\mathrm{d}z \int_{C_{W\pm}} \mathrm{e}^{\pm \mathrm{i}kx} \frac{\partial \chi}{\partial n}\,\mathrm{d}\ell, \tag{B 2}$$

where C_{W+} and C_{W-} are the waterlines along the sidewalls S_{w+} and S_{w-} shown in figure 2. Noting that both $\mathrm{e}^{\pm \mathrm{i}kx}$ and χ satisfy the Helmholtz equation on the free surface S_F shaded in figure 2,

$$(\nabla^2 + k^2)\{\mathrm{e}^{\pm \mathrm{i}kx}, \chi\} = 0 \qquad \text{on} \quad S_F, \tag{B 3}$$

we invoke Green's formula

$$\begin{aligned} 0 &= \iint_{S_F} \{\mathrm{e}^{\pm \mathrm{i}kx}(\nabla^2 + k^2)\chi - \chi(\nabla^2 + k^2)\,\mathrm{e}^{\pm \mathrm{i}kx}\}\,\mathrm{d}S \\ &= \int_{\partial S_F} \left\{ \mathrm{e}^{\pm \mathrm{i}kx} \frac{\partial \chi}{\partial n} - \chi \frac{\partial \mathrm{e}^{\pm \mathrm{i}kx}}{\partial n} \right\} \mathrm{d}\ell, \end{aligned} \tag{B 4}$$

where ∂S_F includes $C_{W\pm}$, the two transverse boundaries $C_{P\pm}$ and the cylinder waterline C_0. It follows from (B 4) that

$$\int_{C_{W\pm}+C_{P\pm}} \left\{ \mathrm{e}^{\pm \mathrm{i}kx} \frac{\partial \chi}{\partial n} - \chi \frac{\partial \mathrm{e}^{\pm \mathrm{i}kx}}{\partial n} \right\} \mathrm{d}\ell = \int_{C_0} \left\{ \mathrm{e}^{\pm \mathrm{i}kx} \frac{\partial \chi}{\partial r} - \chi \frac{\partial \mathrm{e}^{\pm \mathrm{i}kx}}{\partial r} \right\} \mathrm{d}\ell, \tag{B 5}$$

where the integration along C_0 is counter-clockwise. On the line boundaries $C_{W\pm}$,

$$\frac{\partial \mathrm{e}^{\pm \mathrm{i}kx}}{\partial n} = \pm \frac{\partial \mathrm{e}^{\pm \mathrm{i}kx}}{\partial y} = 0.$$

The line integrals along C_{P+} and C_{P-} cancel each other since both $\mathrm{e}^{\pm \mathrm{i}kx}$ and χ and their x-derivatives have equal magnitudes but opposite signs. Therefore, (B 5) reduces to

$$\int_{C_{W\pm}} \mathrm{e}^{\pm \mathrm{i}kx} \frac{\partial \chi}{\partial n}\,\mathrm{d}\ell = \int_{C_0} \left\{ \mathrm{e}^{\pm \mathrm{i}kx} \frac{\partial \chi}{\partial r} - \chi \frac{\partial \mathrm{e}^{\pm \mathrm{i}kx}}{\partial r} \right\} \mathrm{d}\ell. \tag{B 6}$$

Thus the line integral (B 2) along the waterlines of the sidewalls is now reduced to the integral along the waterline of the small cylinder.

We now examine the neighbourhood of the small cylinder. The potential χ in (4.18) can be written as

$$\begin{aligned} \chi &= \frac{\pi}{4}(A^+ + A^-)Y_0(kr_0) - \frac{\mathrm{i}\pi}{2}(A^+ - A^-)Y_1(kr_0)\cos\theta_0 + O((kr_0)^0) \\ &= \frac{1}{2}(A^+ + A^-)\ln kr_0 + \mathrm{i}(A^+ - A^-)\frac{\cos\theta_0}{kr_0} + O((kr_0)^0), \quad kr_0 = O(\mu) \ll 1, \end{aligned} \tag{B 7}$$

where the approximate expressions of Bessel functions for small arguments have been

used. Thus the integral can be approximated by

$$\begin{aligned}\int_{C_0} \chi \frac{\partial e^{\pm ikx}}{\partial r}\,d\ell &= \int_{C_0} \pm ik\cos\theta_0\, e^{\pm ika\cos\theta_0}\chi\,d\ell \\ &= \int_{C_0} \pm ik\cos\theta_0\left\{\frac{A^+ + A^-}{2}\ln ka + i(A^+ - A^-)\frac{\cos\theta_0}{ka} + O(1)\right\}d\ell + O(\mu) \\ &= \int_0^{2\pi} \mp(A^+ - A^-)\cos^2\theta_0\,d\theta_0 + O(\mu) = \mp\pi(A^+ - A^-) + O(\mu), \end{aligned} \tag{B 8}$$

which is contributed by the dominant term $Y_1(kr_0)\cos\theta_0$.

From (B 7), the radial gradient along the circles C_0 pointing out of the fluid domain can be approximated by

$$\left.\frac{\partial\chi}{\partial r}\right|_{C_0} = \frac{(A^+ + A^-)}{2r_0} - (A^+ - A^-)\frac{i\cos\theta_0}{kr_0^2} + O(1), \qquad r_0 = a. \tag{B 9}$$

Thus,

$$\begin{aligned}&\int_{C_0} e^{\pm ikx}\frac{\partial\chi}{\partial r}\,d\ell \\ &= \int_0^{2\pi} e^{\pm ika\cos\theta_0}\left\{\frac{(A^+ + A^-)}{2} - i(A^+ - A^-)\frac{\cos\theta_0}{ka}\right\}d\theta_0 + O(\mu) \\ &= \int_0^{2\pi}(1 \pm ika\cos\theta_0)\left\{\frac{(A^+ + A^-)}{2} - i(A^+ - A^-)\frac{\cos\theta_0}{ka}\right\}d\theta_0 + O(\mu) \\ &= \pi(A^+ + A^-) \pm \pi(A^+ - A^-) + O(\mu) = 2\pi A^\pm + O(\mu). \end{aligned} \tag{B 10}$$

Both $Y_0(kr_0)$ and $Y_1(kr_0)\cos\theta_0$ contribute equally to the integral. By inserting (B 8) and (B 10) into (B 6), it follows that

$$\int_{C_{W\pm}} e^{\pm ikx}\frac{\partial\chi}{\partial n}\,d\ell = \pi(3A^\pm - A^\mp), \tag{B 11}$$

up to the leading order in μ. Substituting (B 11) into (B 2), and then the results (5.2) and (5.3) into Green's formula (5.1), we finally obtain the evolution equations coupling A^+ and A^-,

$$\frac{\partial A^\mp}{\partial t_1} \mp \frac{gk}{\omega}\int_{-H}^0 \left(\frac{Z(z)}{Z(0)}\right)^2 dz\frac{\partial A^\mp}{\partial x_1} = -\frac{\pi i}{2kDW}\frac{gk}{\omega}\int_{-H}^0\left(\frac{Z(z)}{Z(0)}\right)^2 dz(3A^\pm - A^\mp). \tag{B 12}$$

After evaluating the vertical integral

$$\frac{gk}{\omega}\int_{-H}^0\left(\frac{Z(z)}{Z(0)}\right)^2 dz = \frac{gk}{\omega}\int_{-H}^0\frac{\cosh^2 k(z+H)}{\cosh^2 kH}\,dz = \frac{\omega}{2k}\left(1 + \frac{2kH}{\sinh 2kH}\right) = C_g, \tag{B 13}$$

where C_g is the group velocity of a simple progressive wave, (B 12) reduces to (5.4*a*) and (5.4*b*).

REFERENCES

Abramowitz, M. & Stegun, I. A. 1972 *Handbook of Mathematical Functions*. Dover.

Aschcroft, N. W. & Mermin, N. D. 1976 *Solid State Physics*. Thomson Learning Inc.

Bai, K. J. & Yeung, R. 1974 Numerical solutions of free-surface and flow problems. In *Proc. 10th Symp. Naval Hydrodyn.*, pp. 609–641. Office of Naval Research.

Callan, M., Linton, C. M. & Evans, D. V. 1991 Trapped modes in two-dimensional wave guides. *J. Fluid Mech.* **229**, 51–64.

Chen, H. S. & Mei, C. C. 1974*a* Oscillations and wave forces in a man-made harbor in the open sea. In *Proc. 10th Symp. Naval Hydrodyn.* Office of Naval Research.

Chen, H. S. & Mei, C. C. 1974*b* Oscillations and wave forces in an offshore harbor. *Tech. Rep.* 190. Parsons Lab., Massachusetts Institute of Technology.

Cole, J. D. & Kevorkian, J. K. 1981 *Perturbation Methods in Applied Mathematics*. Springer.

Evans, D. V. 1990 The wide-spacing approximation applied to multiple scattering and sloshing problem. *J. Fluid Mech.* **210**, 647–658.

Goo, J.-S. & Yoshida, K. 1990 A numerical method for huge semisubmersible responses in waves. *Soc. Naval Archit. Mar. Engrs Trans.* **98**, 365–387.

Hara, T. & Mei, C. C. 1987 Bragg scattering of surface waves by periodic bars: theory and experiment. *J. Fluid Mech.* **178**, 221–241.

Hu, X. & Chan, C. T. 2005 Refraction of water waves by periodic cylinder arrays. *Phys. Rev. Lett.* **95**, 154501:1–4.

Joannopoulos, J. D., Meade, R. D. & Winn, J. N. 1995 *Photonic Crystals: Molding the Flow of Light*. Princeton University Press.

Kagemoto, H. & Yue, D. K. P. 1986 Interactions among multiple three-dimensional bodies in water waves: an exact algebraic method. *J. Fluid Mech.* **166**, 189–209.

Kajiura, K. 1963 The leading wave of a tsunami. *Bull. Earthquake Res. Inst. Univ. Tokyo* **41**, 525–571.

Kittel, C. 2004 *Introduction to Solid State Physics*, 8th edn. John Wiley & Sons.

Kriegsmann, G. 2004 Complete transmission through a two-dimensional diffraction grating. *SIAM J. Appl. Maths* **65**, 24–42.

Li, Y. 2006 Linear and nonlinear resonance of water waves near periodic structures. PhD thesis, Massachusetts Institute of Technology.

Li, Y. & Mei, C. C. 2006 Subharmonic resonance of a trapped wave near a vertical cylinder in a channel. *J. Fluid Mech.* **561**, 391–416.

Linton, C. M. & Evans, D. V. 1990 The interaction of waves with arrays of vertical circular cylinders. *J. Fluid Mech.* **215**, 549–569.

Linton, C. M. & Evans, D. V. 2001 *Handbook of Mathematical Techniques for Wave/structure Interactions*. Chapman & Hall/CRC.

Linton, C. M. & Martin, P. A. 2004 Semi-infinite arrays of isotropic point scatterers. a unified approach. *SIAM J. Appl. Maths.* **64**, 1035–1056.

Linton, C. M., Porter, R. & Thompson, I. 2007 Scattering by a semi-infinite periodic array and the excitation of surface waves. *SIAM J. Appl. Maths* (submitted).

Linton, C. M. & Thompson, I. 2007 Resonant effects in scattering by periodic arrays. *Wave Motion* **44**, 165–175.

Maniar, H. D. & Newman, J. N. 1997 Wave diffraction by a long array of cylinders. *J. Fluid Mech.* **339**, 309–330.

Martin, P. 2006 *Multiple Scattering: Interaction of Time-harmonic Waves with N Obstacles*. Cambridge University Press.

Maystre, D., Saillard, M. & Tayeb, G. 2001 Special methods of wave diffraction. In *Scattering* (ed. P. Sabatier & E. R. Pike). Academic.

Mei, C. C. 1985 Resonant reflection of surface water waves by periodic sandbars. *J. Fluid Mech.* **152**, 315–335.

Mei, C. C. 1989 *Applied Dynamics of Ocean Surface Waves*. World Scientific.

Mei, C. C., Hara, T. & Naciri, M. 1988 Note on bragg scattering of water waves by parallel bars on the sea bed. *J. Fluid Mech.* **186**, 147–162.

Miles, J. W. 1982 On Rayleigh scattering by a grating. *Wave Motion* **4**, 285–292.

Miles, J. W. & Chamberlain, P. G. 1998 Topographical scattering of gravity waves. *J. Fluid Mech.* **361**, 175–188.

Naciri, M. & Mei, C. C. 1988 Bragg scattering of water waves by a doubly periodic seabed. *J. Fluid Mech.* **192**, 51–74.

Nayfeh, A. H. 1973 *Perturbation Methods*. Wiley.

Ohkusu, M. 1970 On the motion of multihull ships in waves(i). *Rep. Res. Inst. Appl. Mech., Kyushu University* **58**, 167–185.

Peter, M. A. & Meylan, M. H. 2004 Infinite-depth interaction theory for arbitrary floating bodies applied to wave forcing of ice floes. *J. Fluid Mech.* **500**, 145–2167.

Peter, M. A., Meylan, M. H. & Linton, C. M. 2006 Water-wave scattering by a periodic array of arbitrary bodies. *J. Fluid Mech.* **548**, 237–256.

Rey, V., Guazzelli, E. & Mei, C. C. 1996 The effects of oblique incidence and sloping bottom on the bragg resonance were also studied. *Phys. Fluids* **8**, 1525–1530.

Spring, B. H. & Monkmeyer, P. 1974 Interaction of plane waves with vertical cylinders. In *Proc. 14th Coastal Eng. Conf.*, pp. 1828–1847. ASCE.

Srokosz, M. A. & Evans, D. V. 1979 A theory for wave-power absorption by two independently oscillating bodies. *J. Fluid Mech.* **90**, 337–362.

Yariv, A. & Yeh, P. 1984 *Optical Waves in Crystals: Propagation and Control of Laser Radiation*. Wiley-Interscience.

Yue, D. K. P., Chen, H. S. & Mei, C. C. 1978 A hybrid element method for diffraction of water waves by three-dimensional bodies. *Intl J. Numer. Meth. Engng* **12**, 245–266.